ADVANCED FUNCTIONAL MATERIALS
www.afm-journal.de

Materials Views
www.MaterialsViews.com

Acceptor-Substituted *S,N*-Heteropentacenes of Different Conjugation Length: Structure–Property Relationships and Solar Cell Performance

Hannelore Kast, Amaresh Mishra, Gisela L. Schulz, Marta Urdanpilleta, Elena Mena-Osteritz, and Peter Bäuerle**

The synthesis, optoelectronic, and photovoltaic properties of novel acceptor–donor–acceptor (A–D–A) based π-conjugated functional molecules 1–3, comprising a planar *S,N*-heteropentacene as central donor substituted with various terminal acceptor units, such as 1,1-dicyanovinylene (DCV) and 1-(1,1-dicyanomethylene)-cyclohex-2-ene (DCC), are reported. The structural variation of the end groups provides molecules 1–3 with gradually increased π-conjugation due to a rising number of double bonds, which comes from the DCC unit(s). From optoelectronic investigation, structure–property relationships are deduced and the novel A–D–A heteropentacenes 1–3 are implemented as photoactive donor component in solution-processed bulk heterojunction solar cells together with [6,6]-phenyl-C_{61}-butyric acid methyl ester as acceptor. The structural variation in the *S,N*-heteropentacenes leads to clear trends in the photovoltaic performance and power conversion efficiencies of up to 4.9% are achieved. Furthermore, due to extension of the double bonds a clear trade-off between the open circuit voltage (V_{OC}) and the short circuit current density (J_{SC}) values is observed. The role of additives on the optimization of the nanoscale morphology and device performance is investigated. The findings presented herein demonstrate that depending on the types of materials the additive may have significantly different effects on the active layer morphology and the device performance.

1. Introduction

Bulk heterojunction organic solar cells (BHJSC) based on oligomeric donor components, often referred to as "small molecules," and fullerenes as acceptor emerged as competitive alternative to devices prepared from frequently used polymeric counterparts.[1] In single junction solution-processed BHJ solar cells using oligomeric donors as p-type and fullerene derivative as n-type acceptor materials power conversion efficiencies (PCE) over 9% have been achieved.[2] Not only because record PCEs were obtained, but also the structurally defined oligomers possess unique advantages over polymers in terms of synthetic reproducibility and purity leading to well-defined molecular materials with very small batch-to-batch variations.[3] Moreover, they provide the opportunity to develop new understanding of the interrelation between molecular structure and properties to the device performance.[4] In this respect, π-conjugated oligomers built up from alternating electron-rich donor (D) and electron-poor acceptor (A) segments provide excellently performing materials with strong charge transfer character, absorptions in the visible to near-infrared region, lower highest occupied molecular orbital (HOMO)–lowest unoccupied molecular orbital (LUMO) energy gaps, and good charge carrier mobilities.[5] Among them, acceptor–donor–acceptor (A–D–A) oligothiophenes are well developed and the structural principle has often been used to achieve high-performing donor materials in either vacuum[6] or solution-processed[7] organic solar cells. Proper functionalization and substitution in these molecules allow for good processability and control of the electronic energy levels, which not only leads to broad absorption of the solar spectrum, but also to high open circuit voltages (V_{OC}) and excellent stability toward oxidation.

In the search for new organic semiconductors and even stronger absorbers, we recently introduced fused thiophene (S)–pyrrole (N)-based *S,N*-heteroacenes and their acceptor-capped derivatives as the next generation A–D–A-type donor molecules. In this novel class of potential donor materials for OSCs, we were able to combine the favorable properties of oligothiophenes, which exhibit increased stability due to a low lying HOMO energy level, and of oligoacenes typically showing high charge transport properties due to a planar, rigid, and highly conjugated backbone. Corresponding dicyanovinylene (DCV)-substituted

H. Kast, Dr. A. Mishra, Dr. G. L. Schulz, Dr. M. Urdanpilleta, Dr. E. Mena-Osteritz, Prof. P. Bäuerle
Institute of Organic Chemistry II and Advanced Materials
University of Ulm
Albert-Einstein-Allee 11, 89081 Ulm, Germany
E-mail: amaresh.mishra@uni-ulm.de; peter.baeuerle@uni-ulm.de
Dr. M. Urdanpilleta
Department of Applied Physics I
University of the Basque Country (UPV/EHU)
Plaza de Europa 1, 20018 Donostia-San Sebastián, Spain

DOI: 10.1002/adfm.201500565

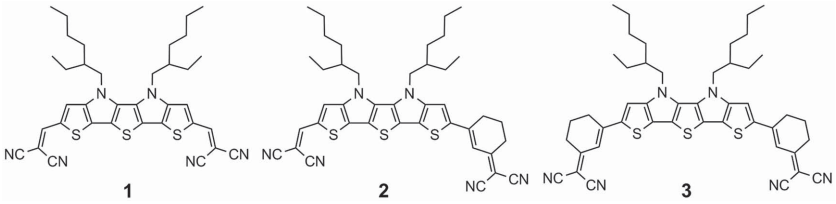

Figure 1. Acceptor-capped *S,N*-heteropentacenes **1–3** comprising DCV and DCC acceptor groups leading to gradually extended conjugated π-systems.

S,N-heterohexacene DCV-SN6 had very intense optical transitions and exhibited good p-channel charge-carrier mobilities of up to 0.02 $cm^2\ V^{-1}\ s^{-1}$ caused by an extended band-like π-conjugated backbone, which comprises substantial quinoidal character and bond length equalization in the ground state.[8] The somewhat smaller, DCV-substituted *S,N*-heteropentacenes DCV-SN5, were implemented in vacuum-processed BHJSCs as donor and C_{60} as acceptor and led to very promising photovoltaic behavior resulting in high V_{OC}'s of up to 0.95 V, fill factors (FF) of up to 0.7, and PCEs of up to 6.5%.[9] Roncali and co-workers have reported the first member of the A–D–A *S,N*-heteroacene series, the DCV-capped dithieno[3,2-*b*:2′,3′-*d*]pyrrole, exhibiting PCE of 0.24% in bilayer solar cells using C_{60} as acceptor.[10]

Sometimes, rigid multifused heteroacene structures have been used as donor block in D–A polymers for efficient polymer bulk heterojunction solar cells,[11] whereas in oligomers they are very scarce. Very recently, Bazan and co-workers implemented a pentafused silaindacenodithiophene unit in a structurally defined D–A–D–A–D molecule and excellent PCEs up to 6.4% have been reached in corresponding solution-processed BHJSCs.[12]

Herein, we now report the development of solution-processable, acceptor-substituted *S,N*-heteropentacenes **1–3** comprising the planar SN5 system as central donor, which was substituted by ethylhexyl side chains in order to provide sufficient solubility. As terminal acceptor we chose on one hand the typical DCV group, which provides perfectly balanced acceptor strength and strong intermolecular interactions in the solid state, but as well introduced 1-(1,1-dicyanomethylene)-cyclohex-2-ene (DCC)[13] to the A–D–A system leading to a gradual extension of the backbone conjugation by one double bond per DCC unit (**Figure 1**). We have recently investigated the influence of the additional *trans*-configurated double bonds in a series of DCC-capped oligothiophenes. In comparison to the DCV derivatives of equal conjugation length improved photovoltaic behavior in vacuum-processed bulk heterojunction solar cells was observed.[14] Thus, the series of novel A–D–A molecules **1–3** allowed to deduce structure–property relationships with respect to the effect of the increasing number of double bonds in the conjugated backbone on optical, electrochemical, and thermal properties. Furthermore, the photovoltaic performance of **1–3** as donor component in solution-processed BHJSCs revealed a clear trend concerning the effective conjugation length in the A–D–A systems.

2. Synthesis

The synthetic routes of A–D–A molecules **1–3** are displayed in **Scheme 1**. The *S,N*-heteropentacene **4** was prepared in 60% yield by tandem Buchwald–Hartwig amination of 3,3′,3″,4′-tetrabromo-2,2′:5′,2″-terthiophene and ethylhexyl amine.[15] Dialdehyde **5**, which was synthesized by Vilsmeier–Haack formylation of **4**, was reacted with malononitrile and β-alanine as catalyst to obtain target DCV end-capped *S,N*-heteropentacene **1** in 86% yield (Scheme 1a).

Synthesis of asymmetric molecule **2** was started by monostannylation of **4** followed by Pd-catalyzed Stille coupling with 3-bromocyclohex-2-enone **7** to afford **8** in 83% yield. Reaction of ketone **8** with malononitrile using equimolar amount of $Ti(O\text{-}iPr)_4$ in a dichloroethane/*i*-propanol[16] solvent mixture afforded mono-DCC derivative **9**. Successive formylation of **9** with *N,N*-dimethylformamide (DMF)/$POCl_3$ gave aldehyde **10**, which was transformed into the corresponding DCV derivative by Knoevenagel condensation with malononitrile and β-alanine to give **2** in 91% yield (Scheme 1b).

For the synthesis of molecule **3**, *S,N*-heteropentacene **4** was first distannylated by lithiation with *n*-BuLi and quenched with trimethyltin chloride (Scheme 1c). Stille coupling of stannyl derivative **11** with 3-bromocyclohex-2-enone afforded diketone **12** in 73% yield. Subsequent Knoevenagel condensation of **12** with malononitrile and $Ti(O\text{-}iPr)_4$ gave after three days of prolonged heating target DCC-capped molecule **3** in about 40% yield together with mono-reacted product. The yield of **3** was increased by further reaction of the mono-substituted derivative with malononitrile in the presence of equimolar amount of $Ti(O\text{-}iPr)_4$.

3. Thermal Properties

The melting points of molecules **1–3** were determined by differential scanning calorimetry (DSC). In the DSC curves, one sharp endothermic peak indicating the melting temperature (T_m) is observed for each molecule. The successive replacement of the terminal DCV by DCC units resulted in melting temperatures of 269 °C for both, **1** and **2**, and 347 °C for **3** (**Figure 2**). Decomposition of the materials started above 360 °C for **1**, above 320 °C for **2**, and above 350 °C for **3**, which is indicated by a broad exothermic peak in the DSC curves.

4. Optical and Electrochemical Properties

The optical properties of all compounds were studied by UV–vis absorption and fluorescence spectroscopy in dichloromethane solution (**Figure 3**) and the data are listed in **Table 1**. In solution DCV derivative **1** showed an intensive charge-transfer absorption band at 582 nm with a high molar extinction coefficient ε of 139 800 $M^{-1}\ cm^{-1}$. After replacing one DCV by a DCC unit in asymmetric *S,N*-heteropentacene **2**, the absorption maximum was red-shifted to 605 nm with a concomitant spectral broadening. Further red-shift and broadening of the absorption band to 632 nm was observed for symmetrical DCC-capped derivative **3**. This strong red-shift of 23 and 50 nm for **2** and **3**, respectively, is attributed to the extension of the π-conjugation by one or two additional double bonds due to the DCC units. Molecules

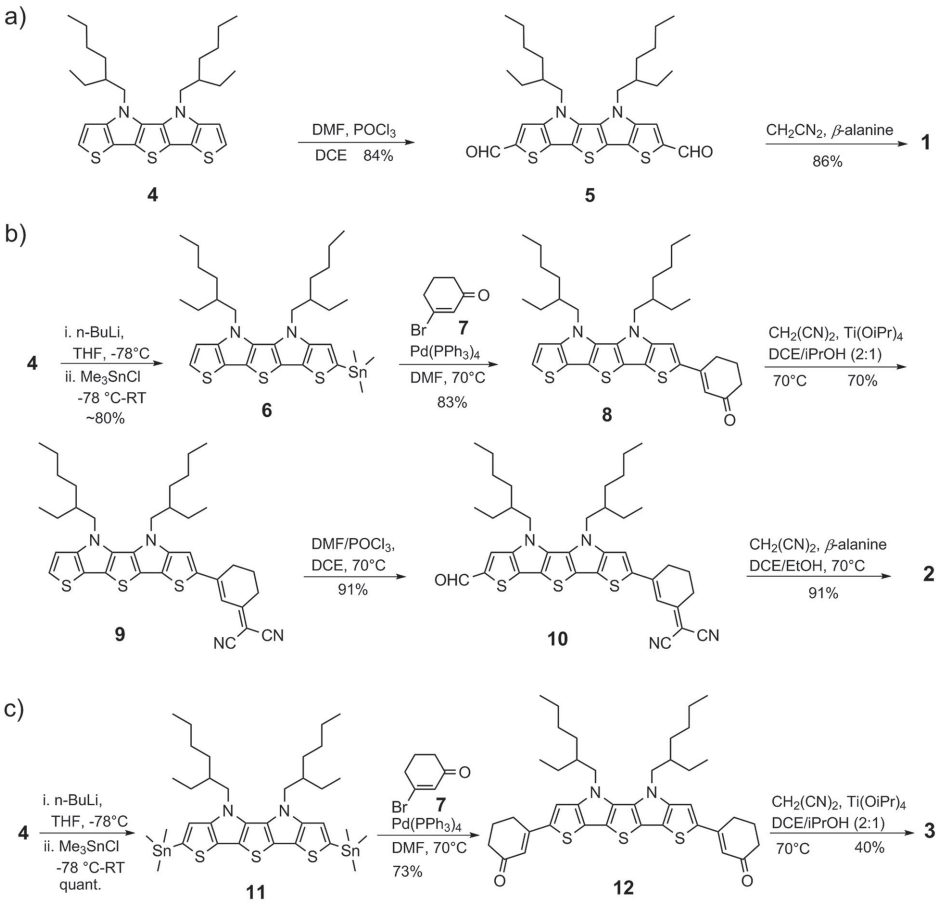

Scheme 1. Synthesis of symmetrical and asymmetrical acceptor-substituted *S*,*N*-pentacenes **1**–**3**.

2 and **3** exhibited an ε of 132 200 and 125 800 M^{-1} cm^{-1}, respectively, which are gradually reduced compared to **1**. The optical HOMO–LUMO gap decreased from 2.01 eV for **1** to 1.90 eV for **2** and to 1.79 eV for **3**.

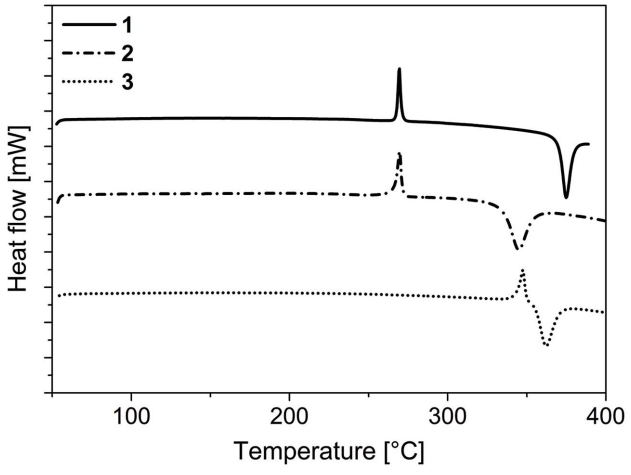

Figure 2. DSC trace of all A–D–A molecules **1**–**3** measured under Ar flow at heating rate of 10 °C min^{-1}.

The emission spectrum of DCV derivative **1** showed a structured band with a maximum at 611 nm and a vibronic shoulder at around 660 nm. Similar to the absorption spectra, the emission spectra of molecule **2** ($\lambda_{max,em}$ = 677 nm) and **3** ($\lambda_{max,em}$ = 703 nm) were red-shifted and broadened. All molecules showed relatively small Stokes shifts between 703 and 1454 cm^{-1} indicating a stiff and planar conjugated π-system. Compared to molecule **1**, the increased Stokes shift for **2** and **3** is due to higher molecular flexibility originating from the terminal DCC units.

Compared to the solution spectra, the absorption bands of **1**–**3** in thin films were red-shifted and significantly expanded toward lower energies (**Figure 4**) which is important for the improvement of the spectral overlap with the solar emission spectrum when applied in OSCs. All films showed vibronic progression at longer wavelengths which is accounted to intermolecular π–π interactions of the planar molecular backbones. The optical HOMO–LUMO gaps of the molecules in thin films determined from the absorption band edge decreased from 1.79 eV for **1** to 1.65 eV for **2** and to 1.56 eV for **3** as a result of the elongation of the π-system.

Electrochemistry was performed in order to determine HOMO and LUMO energy levels. **Figure 5** shows cyclic voltammograms of molecules **1**–**3** and the data are summarized

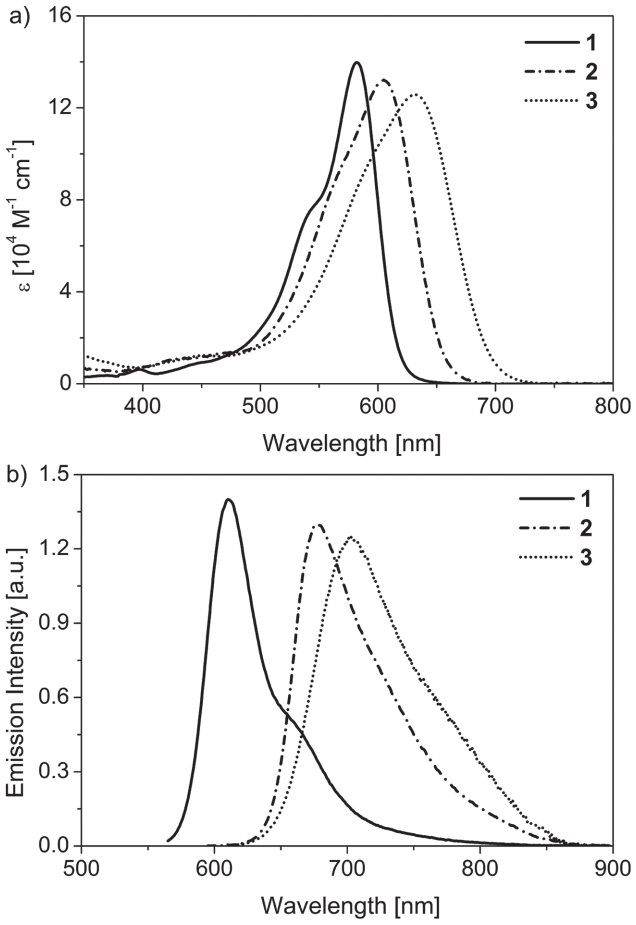

Figure 3. a) UV–vis and b) fluorescence spectra of SN5-derivatives **1**–**3** measured in dichloromethane at 25 °C.

in **Table 2**. Typically, two reversible one-electron oxidation ($2 \times 1e^-$) processes occurred, which are assigned to the formation of stable *S,N*-heteropentacene radical cations and dications. Compared to molecule **1**, the successive replacement of the DCV units by DCC groups in **2** and **3** resulted in a lowering of the oxidation potential by 0.18 and 0.32 V, respectively, indicating an increasing conjugated π-system caused by the additional double bond of the DCC units.

In the negative potential regime, *S,N*-heteropentacenes **1** and **2** showed two irreversible reduction processes. While, for DCC-capped derivative **3** a reversible wave comprising a one $2e^-$ process was observed indicative for the formation of a stable radical anion on each DCC unit. At the same time, the reduction potentials were cathodically shifted with increasing number of DCC units. In these multifused systems, the acceptor units are separated from one another by rigid heteropentacene moiety. This introduces enhanced conformational rigidity to these molecules and permits greater electronic communication between the chromophores leading to the separation of the reduction waves in case of **1** and **2**. By going from **1** to **3** the gap between the reduction waves decreases and finally a single reduction process was observed for DCC derivative **3**. The HOMO and LUMO energy levels of the three molecules were calculated from the onset of the first oxidation and reduction wave. An increase in HOMO and as well in LUMO energy level is observed for molecules **1**–**3** concomitant with the extension of p-conjugation by one or two additional double bonds. Because of both effects, the resulting electrochemical gap (ΔE_{CV}) was reduced from 1.82 eV for **1** to 1.74 eV for **2** and to 1.67 eV for **3** in good agreement with the optical gaps (ΔE_{opt}). On the basis of electrochemical measurements one should expect higher open circuit voltage (V_{OC}) for compound **1** in solar cells due to its deepest HOMO energy level among all three derivatives. On the other hand, the broad absorption profile of **3** should be beneficial for achieving higher short circuit current (J_{SC}).

5. Photovoltaics Properties

Solution-processed BHJ solar cells were prepared by spin-coating blends of **1**–**3** as electron donors and [6,6]-phenyl-C_{61}-butyric acid methyl ester ($PC_{61}BM$) as electron acceptor using chloroform ($CHCl_3$) as processing solvent. The optimized blend ratio was individually determined for each derivative together with investigating a range of device fabrication parameters (e.g., spin speed, solution concentration, or the use of solvent additives). The device structure was indium tin oxide (ITO)/PEDOT:PSS/donor:$PC_{61}BM$/LiF/Al. The photoactive layer thickness of the optimized devices for compound **1** is 40 ± 5 nm and for compound **2** and **3** is about 65 ± 5 nm. The current density–voltage (*J*–*V*) characteristics and external quantum efficiency (EQE) spectra of the optimized devices for **1**–**3** are shown in **Figure 6**a,b. The solar cell data for all compounds are summarized in Table 2.

The devices based on **1**:$PC_{61}BM$ (2:3 w/w) exhibited a high open circuit voltage (V_{OC}) of 1.10 V, a short-circuit current density (J_{SC}) of 3.4 mA cm^{-2}, a fill factor (FF) of 0.42, and a PCE of 1.6%. The solar cell performance was further examined by using solvent additives, such as, chloronaphthalene (CN) and diiodoctane (DIO). In OSCs, the use of processing additives has proven to be an effective way to tailor the nanoscale morphology

Table 1. Optical and electrochemical data of *S,N*-heteropentacenes **1**–**3**.

Molecules	λ_{abs} sol[a] [nm]	ε [M^{-1} cm^{-1}]	ΔE_{opt} sol[a] [eV]	λ_{em} sol [nm]	Stokes shift [cm^{-1}]	λ_{abs} film[b] [nm]	ΔE_{opt} film [eV]	E°_{ox1} [V]	E°_{ox2} [V]	E°_{red1} [V]	HOMO[b] [eV]	LUMO[b] [eV]	ΔE_{CV}[c] [eV]
1	582	139 800	2.01	611	703	592, 630	1.79	0.64	1.27	–1.33	–5.67	–3.85	1.82
2	605	132 200	1.90	677	1454	625, 680	1.65	0.46	1.04	–1.44	–5.48	–3.74	1.74
3	632	125 800	1.79	703	1201	638, 718	1.56	0.32	0.94	–1.48	–5.35	–3.68	1.67

[a]Absorption measured in dichloromethane; [b]Film spin-coated from chloroform solution; [c]The redox potentials (E°_{ox} and E°_{red}) were calculated by the mean of the cathodic and anodic peak potentials of quasi-reversible waves: $E^{\circ} = (E_{pa} + E_{pc})/2$. For the irreversible waves, the redox potentials E° were determined at $I_0 = 0.855 I_p$.[17]

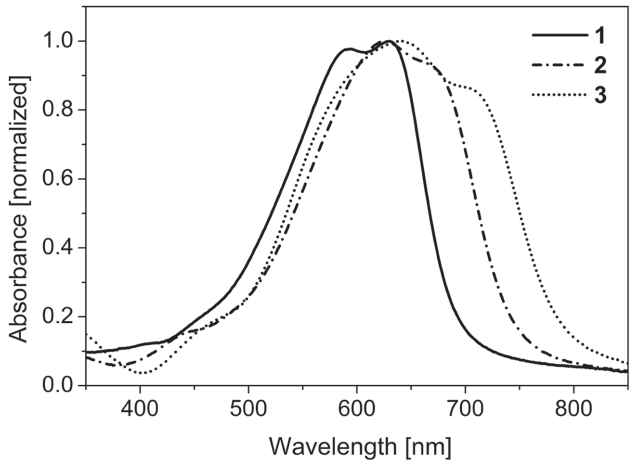

Figure 4. Thin film UV–vis spectra of SN5 derivatives **1**–**3** deposited by spin-coating on glass substrates.

of active layers leading to improved charge collection and transport properties. The role of additives on solar cell performance was first demonstrated in polymer-based devices[18] and recently have been widely investigated in small molecule–based devices.[19] The use of CN and DIO in chloroform resulted in an improved performance mostly due to an increase in the charge transport properties as reflected in the higher J_{SC} values of 6.4 and 4.5 mA cm^{-2}, respectively. We found that in the active layer the donor/acceptor components can phase separate in the presence of additives into an optimum morphology for balanced charge transport which was probed by atomic force microscopy (vide infra). As CN seems to be more promising, the devices were further optimized by varying the additive concentration in chloroform and the best result was achieved with 7 mg mL^{-1} CN (Table S1, Supporting Information). The device generated a J_{SC} of 6.4 mA cm^{-2} and a slightly higher V_{OC} of 1.13 V, an FF of 0.43 resulting in a twofold increase in efficiency to 3.1%. The

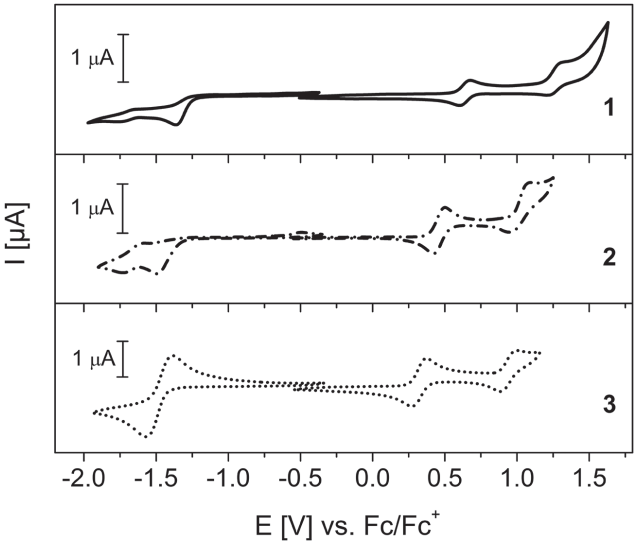

Figure 5. Cyclic voltammograms of SN5- derivatives **1**–**3** measured in dichloromethane at 25 °C, supporting electrolyte $TBAPF_6$ (0.1 M), scan rate 100 mV s^{-1}, potentials versus Fc/Fc$^+$.

average PCE of seven identical devices using CN as additive is 3.0 ± 0.1%. The *J*–*V* curves for the best performing devices with and without CN are shown in Figure S1 (Supporting Information) and the dependence of the PCE on the CN content in Figure S3a (Supporting Information). The device using DIO as an additive generated a higher PCE of 2.1% compared to device without additive. The saturation of the photocurrent (defined as $J_{(-1V)}/J_{SC}$) with the reverse bias is given in Table 2. The devices without additive showed a saturation value of 1.51 indicating a large recombination at short circuit conditions and in reverse bias. While in the presence of CN and DIO as additives the saturation value is significantly reduced to 1.22 and 1.36, respectively, indicating a reduction of the recombination losses and increased charge collection.[20,21]

Replacing one of the DCV groups with a DCC unit in **2** led to a significant increase in the J_{SC} value to 7.6 mA cm^{-2} concurrent with a decrease in V_{OC} to 0.95 V. The **2**:$PC_{61}BM$ (2:3 w/w) device generated an enhanced PCE of 3.0%. The use of CN as additive only slightly improved the efficiency to 3.2%. For **2**:$PC_{61}BM$ devices, DIO turned out to be the best additive with an optimal content of 8.75 mg mL^{-1}. General trends show that the increase in the DIO content from 5 to 8.75 mg mL^{-1} resulted in an increase in the J_{SC} values from 7.6 to 9.4 mA cm^{-2}, while a further increase in the DIO content resulted in a lowering of the J_{SC} value (Table S1, Supporting Information). The *J*–*V* curve for the best performing device with and without DIO is shown in Figure S2 (Supporting Information) and the dependence of PCE with the DIO content in Figure S3b (Supporting Information). The PCE increased from 3.0% to 4.2% by varying the DIO content from 0 to 8.75 mg mL^{-1}. Upon further increase of DIO in chloroform to 10 mg mL^{-1}, a slight decrease in PCE to 4.1% was observed (Table S1, Supporting Information). For the optimized **2**:$PC_{61}BM$ device an increase in both J_{SC} (9.4 mA cm^{-2}) and FF (0.47) led to an increase in the PCE to 4.2% with an average value of 4.1 ± 0.1%. The saturation value for **2**:$PC_{61}BM$ devices also reduced from 1.23 for devices without additive to 1.20 and 1.16 for the use of CN and DIO as additives. In contrast, for the symmetrical DCC-substituted donor molecule **3** the best results were obtained with a D:A ratio of 1:1 without any additional additives. The photovoltaic results with different D:A ratios are presented in Table S2 (Supporting information). The devices with **3**:$PC_{61}BM$ (1:1 w/w) generated a significantly higher J_{SC} of 10.8 mA cm^{-2} and an FF value of 0.51, while the V_{OC} was reduced to 0.88 V giving rise to the highest PCE of 4.9% in the series. The average PCE on a batch of ten identical devices for donor molecule **3** is 4.6 ± 0.2%. A comparatively higher FF and significant lowering of the saturation value to 1.10 for **3**:$PC_{61}BM$ devices are a further indication of efficient charge separation and extraction. The significant increase of J_{SC} can be ascribed to the bathochromic shift and broadening of the absorption spectrum resulting in a better spectral overlap with the solar emission spectrum. The use of CN and DIO as additives led to reduced efficiencies of 3.9% mostly due to a decrease of the J_{SC} values.

The statistical data on a batch of several identical devices for acceptor-capped *S*,*N*-heteropentacenes **1**–**3** with and without additives are summarized in Tables S3–S5 (Supporting information). The small standard deviation in all cases points toward good device reproducibility.

Table 2. Photovoltaic data of SN5-heteropentacenes **1**–**3**.

Donor	Solvent	D:A ratio	J_{SC} [mA cm^{-2}]	V_{OC} [V]	FF	PCE [%]	$J(-1V)/J_{SC}$[a)]	EQE_{max} [%] (@ λ [nm])
1	$CHCl_3$	2:3	3.4	1.10	0.42	1.6	1.51	25 (630)
1	$CHCl_3$/CN (7 mg mL^{-1})	2:3	6.4	1.13	0.43	3.1	1.22	45 (590)
1	$CHCl_3$/DIO (5 mg mL^{-1})	1:1	4.5	1.11	0.41	2.1	1.36	–
2	$CHCl_3$	2:3	7.6	0.95	0.42	3.0	1.23	46 (620)
2	$CHCl_3$/CN (5 mg mL^{-1})	2:3	7.8	0.94	0.43	3.2	1.20	52 (620)
2	$CHCl_3$/DIO (8.75 mg mL^{-1})	2:3	9.4	0.95	0.47	4.2	1.16	54 (640)
3	$CHCl_3$	1:1	10.8	0.88	0.51	4.9	1.10	56 (670)
3	$CHCl_3$/CN (5 mg mL^{-1})	1:1	8.8	0.86	0.52	3.9	1.12	45 (660)
3	$CHCl_3$/DIO (5 mg mL^{-1})	1:1	9.2	0.90	0.47	3.9	1.14	50 (670)

[a)] Defined as $J_{(-1V)}/J_{SC}$.

The comparison of the optimized devices reveals that in the series **1**–**3** the PCE increases from 3.1% to 4.9% which is consistent with the extension of the π-conjugation by the additional double bonds in the DCC acceptor units. The improvement in PCE comes from the gradual increase in J_{SC} and FF, despite a simultaneous decrease of the V_{OC} (Figure 6a). The trade-off between the V_{OC} and J_{SC} values is attributed to the stepwise reduction in the HOMO–LUMO energy gap. The lowering of the V_{OC} values from **1** (1.13 V) to **2** (0.95 V) to **3** (0.88 V) is explained by the gradually raising HOMO energy levels due to the increased conjugation. In general, V_{OC} correlates with the energetic difference between HOMO of the donor molecules and the LUMO of the acceptor $PC_{61}BM$ (–4.0 eV[22].[23] It has also been demonstrated that an energy offset (ΔE_{LL}) of 0.3–0.5 eV between the LUMO of the donor and the LUMO of the acceptor is sufficient to dissociate excitons into free charges.[24] For our series **1**–**3**, we calculate a consistent energetic loss of 0.54–0.47 eV. The increase of the J_{SC} values also becomes evident in the EQE spectra, in which successively the maxima are redshifted (590–670 nm) for the best devices and increased (45%–56%) on going from **1** to **3** (Figure 6b). The shapes of the EQE spectra match perfectly with those of the UV–vis absorption spectra in films. The J_{SC} values obtained from the integration of EQE spectra (6.5 mA cm^{-2} for **1**, 10.6 mA cm^{-2} for **2**, and 11.7 mA cm^{-2} for **3**) were in reasonable agreement with that measured from the *J*–*V* curve.

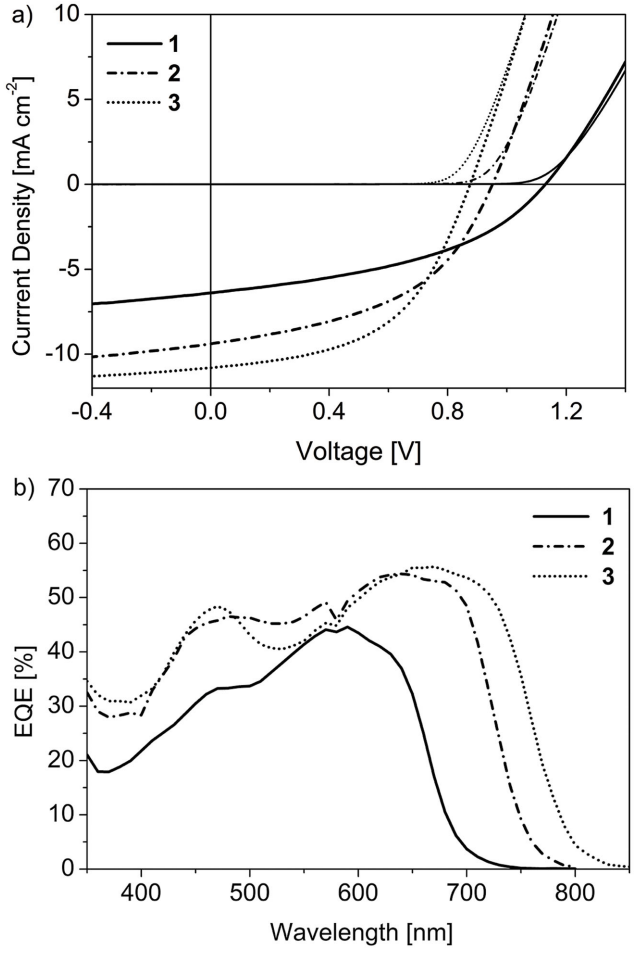

Figure 6. a) *J*–*V* characteristics and b) external quantum efficiency (EQE) spectra of the optimized bulk heterojunction solar cells prepared with **1**–**3** as donor and $PC_{61}BM$ as acceptor.

The overall performance of our *S*,*N*-heteropentacenes **1**–**3** is remarkable, because per se they represent relatively "small" A–D–A molecular materials which is comparable to some of other well-performing solution-processed low molecular weight donor materials, such as smaller squaraines (PCE ≤ 5.2%),[25] diketopyrrolopyrroles (PCE ≤ 4.8%),[26] quinquethiophenes (PCE ≤ 4.6%),[27] merocyanines (PCE ≤ 4.5%),[28] and triarylamine derivatives (PCE ≤ 4.0%).[29]

Atomic force microscopy (AFM) measurements were conducted to characterize the surface morphology of the active organic layers in the photovoltaic devices. Blends of compounds **1**, **2**, and **3** with $PC_{61}BM$ (ratios 2:3, 2:3, and 1:1) were deposited onto a PEDOT:PSS-modified ITO electrode under the same conditions as the corresponding photovoltaic devices. All blends deposited from chloroform solutions showed low topographic roughness of 3 nm for **1** and **2** and 6 nm for **3**. The photoactive layers of **1** and **2** gave evidence to a grain-like structure with grain dimensions of 10–30 and 10–20 nm, respectively (**Figure 7**a,b). On the contrary, blends of **3**:$PC_{61}BM$

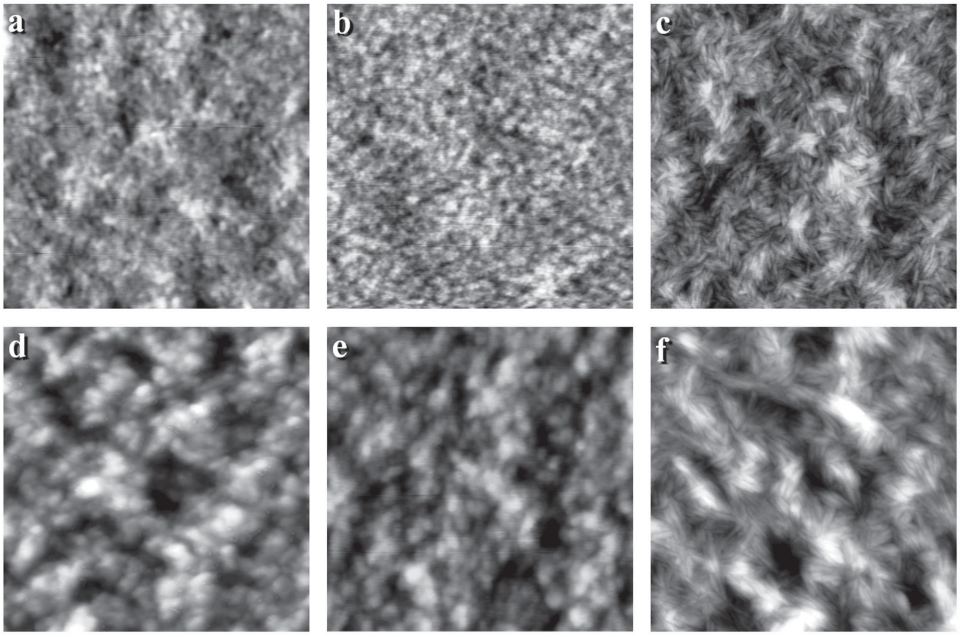

Figure 7. AFM topography images of donor:$PC_{61}BM$ blend films without additive spin-coated on PEDOT:PSS| ITO electrode: a) **1** (Δz = 3 nm), b) **2** (Δz = 4 nm), and c) **3** (Δz = 6 nm). AFM topography images of blend films with additive: d) **1** + CN (Δz = 15 nm), b) **2** + DIO (Δz = 10 nm), and c) **3** + DIO (Δz = 22 nm). Image size: 1 μm × 1 μm.

form needle-like structures of 10–15 nm width and up to 80 nm length (Figure 7c). The corresponding phase images (Figure S4, Supporting Information) do not reveal a clear contrast and therefore no assessment about phase separation is possible at this point. The treatment with additives (CN for **1**; DIO for **2** and **3**) influenced in all cases the film characteristics by increasing the topography roughness of the surface to 15, 10, and 22 nm (Figure 7d,e). After the addition of additive, the grain-like structure of **1** and **2** evolved to larger aggregates (40–80 nm) and a better contrast in the phase images can be obtained ($\Delta\phi$ of 90° and 30°, Figure S4, Supporting Information).

These findings account for a better structured film and clear phase separation by the use of additives which correlates well with the enhancement of the photovoltaic performance in both cases. The film of blend **3**:$PC_{61}BM$ after addition of DIO exhibited comparable needle-like structures as before, acommpanied by a strong increase in the topography roughness (Figure 7f). This effect can explain the reduced efficiency of **3**-based photovoltaic devices upon DIO addition.

6. Conclusion

We have designed and synthesized a new family of small molecule donors **1**–**3** composed of *S,N*-heteropencene as a rigid donor and DCV and DCC as acceptor moieties for application in BHJ solar cells. Replacement of the DCV with DCC unit was found to red-shift and broaden the absorption spectra in solution and thin films as well to raise the HOMO energy level significantly compared to the LUMO level resulting in a material with a lower HOMO–LUMO energy gap. BHJ solar cells were fabricated by solution-processing using these molecules as the electron donor and $PC_{61}BM$ as the electron acceptor. All these small molecules show high PCEs, ranging from 3.1% to 4.9%, and the highest PCE of 4.9% was achieved for a **3**:$PC_{61}BM$ (w:w, 1:1) based device without any additive treatment. On the other hand, the highest PCEs for **1** and **2** were achieved by using either chloronapthalene or diiodooctane as additives. The additive had a significant effect in altering the nanomorphology of the photoactive layer as investigated by AFM. In BHJ devices, the V_{OC} value was significantly decreased from 1.13 V for **1** to 0.88 V for **3** by sequential extension of the backbone conjugation by additional double bond of the DCC unit(s), while an increase in the J_{SC} value from 6.4 mA cm^{-2} for **1** to 10.8 mA cm^{-2} for **3** was observed due to the extended absorption to the NIR region. The results clearly demonstrated that the structural modulation of terminal acceptor units gave an evident trade-off between the V_{OC} and J_{SC} values. Our studies indicate that the planar *S,N*-heteroacene unit is a promising building block for the construction of molecular donors with improved material properties for efficient small molecule OSCs.

7. Experimental Section

Instrument and Measurements: NMR spectra were recorded on a Bruker DRX 400 spectrometer (^{1}H NMR: 400 MHz, ^{13}C NMR: 100 MHz). Chemical shift values (δ) are expressed in parts per million using residual solvent protons (^{1}H NMR: δ_H = 7.26 for $CDCl_3$; δ_H = 5.32 for CD_2Cl_2; δ_H = 1.72 for THF-d8; ^{13}C NMR: δ_C = 77.0 for $CDCl_3$; δ_C = 54.0 for CD_2Cl_2) as internal standard. The splitting patterns are designated as follows: s (singlet), d (doublet), t (triplet), and m (multiplet). Elemental analyses were performed on an Elementar Vario EL. Melting points were determined using a Mettler Toledo DSC 823 or a Büchi Melting Point B-545. Thin layer chromatography was carried out on aluminum plates, precoated with silica gel, Merck Si60 F254. Preparative column chromatography was performed on glass columns packed with silica gel, Merck Silica 60, particle size 40–63 μm or packed with basic alumina

II. High-resolution MALDI-TOF mass spectra (HRMS) experiments were performed using a MS Bruker Reflex 2 (Bruker Daltonik GmbH, Bremen, Germany) using *trans*-2-[3-(4-*tert*-butylphenyl)-2-methyl-2-propenylidene]malononitrile (DCTB) as matrix. UV–vis absorption spectra were recorded on a Perkin Elmer Lambda 19 spectrometer. Cyclic voltammetry experiments were performed with a computer-controlled Autolab PGSTAT30 potentiostat in a three-electrode single-compartment cell with a platinum working electrode, a platinum wire counter electrode, and an Ag/AgCl reference electrode. All potentials were internally referenced to the ferrocene/ferrocenium couple. Surface images of the photoactive layers were recorded with the help of a Bruker MultiMode V AFM with Nanoscope controller at ambient temperature in tapping mode. The images were analyzed using the WSxM software.[30]

Device Fabrication and Photovoltaic Characterization: Photovoltaic devices were made by spin-coating PEDOT:PSS (Clevios P, VP Al4083) onto precleaned, patterned ITO substrates (15 Ω square^{-1}) (Kintec). The photoactive layer was deposited by spin-coating donor **1**–**3** and $PC_{61}BM$ ([6,6]-phenyl-C_{61}-butyric acid methyl ester, Solenne BV, Netherlands) from chloroform solutions (total concentration = 15 mg mL^{-1}) with or without additives leading to layer thicknesses of ≈35–70 nm. The additives CN and DIO were purchased from Sigma-Aldrich and distilled prior to use. The devices for **1** were fabricated by spin-coating at room temperature. For devices containing **2** and **3**, the blend solutions and substrates were heated to 60 °C. The counter electrode of LiF (1 nm) and aluminum (100 nm) was deposited by vacuum evaporation at 2×10^{-6} Torr. The active areas of the cells were 0.2 cm^2. Film thicknesses were measured using a Dektak profilometer. *J–V* characteristics were measured under AM 1.5G conditions at 100 mW cm^{-2} with a AAA solar simulator from Oriel Instruments, using a Keithley 2400 source meter. Spectral response was measured under monochromatic light from a 300 W Xenon lamp in combination with monochromator (Oriel, Cornerstone 260), modulated with a mechanical chopper. The response was recorded as the voltage over a 220 Ω resistance using a lock-in amplifier (Merlin 70104). A calibrated Si cell was used as reference. The devices were kept behind a quartz window in a nitrogen filled container.

Materials: Tetrahydrofuran (THF) and DMF (Merck) were absoluted via MB SPS-800 solvent purifying system (MBraun). All synthetic steps were carried out under argon atmosphere. *n*-Butyl lithium (1.6 M in *n*-hexane) was purchased from Acros, trimethyltin chloride and titanium isopropoxide (Ti(O-*i*Pr)$_4$) were purchased from Sigma-Aldrich, malononitrile and β-alanine were purchased from Merck. Dichloroethane (DCE), dichloromethane (DCM), ethyl acetate (EtOAc), diethyl ether (Et_2O), methanol (MeOH), and ethanol (EtOH) were purchased from VWR international.

*4,5-(Di-2-ethylhexyl)-dithieno[2,3-d:2′,3′-d′]thieno[3,2-b:4,5-b′]dipyrrole]-2,7-dicarbaldehyde (**5**)*: A mixture of $POCl_3$ (746 µL, 8 mmol) and dry DMF (616 µL, 8 mmol) in 10 mL of DCE was stirred for 2 h at room temperature. Then 4,5-(di-2-ethylhexyl)-dithieno[2,3-*d*:2′,3′-*d*′]thieno[3,2-*b*:4,5-*b*′]dipyrrole **4** (200 mg, 0.4 mmol) dissolved in 20 mL of DCE was added and the mixture was stirred at 80 °C for 20 h. Saturated $NaHCO_3$ solution and DCM were added for hydrolysis. The product was extracted with DCM, washed with water, and dried over Na_2SO_4. After removal of the solvent the crude product was purified by column chromatography (SiO_2, DCM) to obtain **5** (186 mg, 0.34 mmol, 84%) as an orange solid. M_p 206 °C (DSC). ^{1}H NMR (400 MHz, $CDCl_3$, δ ppm): 9.90 (s, 2H, —C*H*O), 7.65 (s, 2H, Th-β-*H*), 4.38–4.26 (m, 4H, N—CH_2), 2.03–1.94 (m, 2H, N—CH_2—C*H*), 1.30–1.15 (m, 16H, 4(—CH_2—)), 0.86–0.78 (m, 12H, CH_3). ^{13}C NMR (100 MHz, $CDCl_3$, δ ppm): 182.69, 145.08, 145.06, 140.68, 133.57, 124.54, 119.87, 119.57, 53.31, 40.55, 30.13, 30.08, 28.27, 28.18, 23.50, 23.47, 22.91, 22.88, 13.85, 13.84, 10.51, 10.45. HRMS (MALDI-TOF) *m*/*z*: [M]$^+$ calcd for $C_{30}H_{38}N_2O_2S_3$, 554.20899; found, 554.20848 (δ*m*/*m* = 0.09 ppm). Anal. calcd for $C_{30}H_{38}N_2O_2S_3$: C 64.94, H 6.90, N 5.05; found: C 65.17, H 7.13, N 4.91.

*[4,5-(Di-2-ethylhexyl)-dithieno[2,3-d:2′,3′-d′]thieno[3,2-b:4,5-b′]dipyrrole]-2,7-bis[methan-1-yl-1-ylidene]dimalonodinitrile (**1**)*: Dialdehyde **5** (100 mg, 0.18 mmol), malononitrile (95 mg, 1.44 mmol), and β-alanine (0.96 mg, 10.8 µmol) were dissolved in 30 mL of DCE: EtOH (1:1). The solution was heated at 80 °C for 2 d. After the reaction mixture was allowed to cool to room temperature the solvent was removed and the residue was recrystallized from DCM/*n*-hexane. The solid was filtered off and washed with Et_2O, water, and MeOH. Final purification by column chromatography (SiO_2, DCM) yielded product **1** (100 mg, 0.15 mmol, 86%) as a green solid. M_p 268 °C (DSC). ^{1}H NMR (400 MHz, $CDCl_3$, δ ppm): 7.73 (s, 2H, vinyl-H), 7.71 (s, 2H, Th-β-H), 4.38–4.25 (m, 4H, N—CH_2), 2.01–1.91 (m, 2H, N—CH_2—CH), 1.28–1.17 (m, 16H, 4(—CH_2—)), 0.88–0.79 (m, 12H, CH_3). ^{13}C NMR (100 MHz, $CDCl_3$, δ ppm): 150.26, 146.54, 134.50, 133.48, 126.89, 121.43, 119.38, 114.82, 114.32, 73.76 53.51, 40.63, 30.13, 30.10, 28.28, 28.20, 23.50, 22.92, 22.89, 13.84, 10.49, 10.45. HRMS (MALDI-TOF) *m*/*z*: [M]$^+$ calcd for $C_{36}H_{38}N_6S_3$, 650.23146; found, 650.23104 (δ*m*/*m* = 0.6 ppm). Anal. calcd for $C_{36}H_{38}N_6S_3$: C 66.43, H 5.88, N 12.91, S 14.78; found: C 66.28, H 5.89, N 12.78, S 14.62.

*4,5-(Di-2-ethylhexyl)-2-(trimethylstannyl)-dithieno[2,3-d:2′,3′-d′]thieno[3,2-b:4,5-b′]dipyrrole (**6**)*: 4,5-(Di-2-ethylhexyl)-dithieno[2,3-*d*:2′,3′-*d*′]thieno[3,2-*b*:4,5-*b*′]dipyrrole **4** (294 mg, 0.59 mmol) was dissolved in 18 mL of dry THF under argon and cooled to −78 °C. Then *n*-BuLi (1.6 M in *n*-hexane, 0.37 mL, 0.59 mmol) was added within 35 min. The reaction mixture was stirred for 1 h at −78 °C and then quenched with trimethyltin chloride (182 mg, 0.91 mmol) in 1 mL dry THF. The cooling bath was removed after 5 min and stirring was continued for overnight at room temperature. Water was added to the reaction mixture and the product was extracted with Et_2O. ^{1}H-NMR confirmed a conversion of **6** in about 80%. ^{1}H-NMR (400 MHz, THF-d8, δ ppm): 7.13 (s, 1H, Th-β-*H*), 7.10 (d, *J* = 2.0 Hz, 2H, Th-α-*H*, Th-β-*H*), 4.38–4.33 (m, 4H, N—CH_2), 2.06–2.01 (m, 2H, N—CH_2—C*H*), 1.26–1.15 (m, 16H, 4(—CH_2—)), 0.84–0.76 (m, 12H, CH_3), 0.38 (s, 9H, Sn—CH_3). Compound **6** was used without any further purification.

*3-[4,5-(Di-2-ethylhexyl)-dithieno[2,3-d:2′,3′-d′]thieno[3,2-b:4,5-b′]dipyrrole-2,7-diyl]cyclohex-2-en-1-one (**8**)*: Monostannylated heteropentacene **6** (320 mg, 0.48 mmol) and 3-bromocyclohex-2-*en*-1-one **7** (124 mg, 0.71 mmol) were dissolved in 5 mL of dry DMF and degassed five times before $Pd(PPh_3)_4$ catalyst (23.3 mg, 20.2 µmol) was added. The reaction mixture was stirred at 80 °C for 18 h. After removal of DMF, the reaction mixture was extracted with DCM and washed with water and dried over Na_2SO_4. After evaporation of the solvent the crude product was purified by column chromatography (basic Al_2O_3, DCM) to afford product **8** (235 mg, 0.396 mmol, 83%) as a red solid. M_p 92 °C (DSC). ^{1}H-NMR (400 MHz, CD_2Cl_2, δ ppm): 7.36 (s, 1H, Th-β-*H*), 7.16 (d, *J* = 5.3 Hz, 1H, Th-α-*H*)), 7.05 (d, *J* = 5.3 Hz, 1H, Th-β-*H*)), 6.38 (s, 1H, =C*H*), 4.37–4.23 (m, 4H, N—CH_2), 2.86 (t, *J* = 5.8 Hz, 2H, cyclo-CH_2), 2.46–2.43 (m, 2H, cyclo-CH_2), 2.18–2.12 (m, 2H, cyclo-CH_2), 2.04–1.99 (m, 2H, N—CH_2–C*H*), 1.26–1.17 (m, 16H, 4(—CH_2—)), 0.85–0.77 (m, 12H, CH_3). ^{13}C-NMR (100 MHz, CD_2Cl_2, δ ppm): 198.62, 153.84, 146.02, 146.00, 145.05, 145.03, 138.33, 133.04, 130.24, 123.49, 120.46, 119.94, 118.63, 116.77, 116.40, 112.33, 112.15, 40.91, 40.85, 37.74, 30.48, 30.44, 30.42, 30.38, 28.69, 28.66, 28.59, 28.57, 28.17, 23.85, 23.82, 23.37, 23.34, 23.31, 23.01, 14.08, 14.06, 14.03, 10.75, 10.71, 10.69, 10.65. HRMS (MALDI-TOF) *m*/*z*: [M]$^+$ calcd for $C_{34}H_{44}N_2OS_3$, 592.26103; found, 592.26107 (δ*m*/*m* = 0.07 ppm).

*2-[3-{4,5-(Di-2-ethylhexyl)-dithieno[2,3-d:2′,3′-d′]thieno[3,2-b:4,5-b′]dipyrrole-2,7-diyl}cyclohex-2-enylidene]malononitrile (**9**)*: Ketone **8** (115 mg, 194 µmol) was dissolved in 4 mL of DCE:*i*-propanol (2:1) in a schlenk tube. After addition of malononitrile (96 mg, 1.45 µmol) and Ti(O-*i*Pr)$_4$ (60 µL, 197 µmol) the reaction mixture was stirred at 70 °C for 2 d. The reaction mixture was diluted with DCM and stirred with 1 M HCl for 1 h. The aqueous phase was removed and the organic phase was washed with saturated $NaHCO_3$ solution and dried over Na_2SO_4. After removal of the solvent by rotary evaporator, the residue was purified by column chromatography (SiO_2, DCM) to obtain product **9** (87 mg, 0.136 mmol, 70%) as a green solid. M_p 229–230 °C. ^{1}H-NMR (400 MHz, CD_2Cl_2, δ ppm): 7.44 (s, 1H, Th-β-H), 7.20 (d, *J* = 5.3 Hz, 1H, Th-α-H), 7.10 (s, 1H, =CH), 7.05 (d, *J* = 5.3 Hz, 1H, Th-β-H), 4.36–4.23 (m, 4H, N—CH_2), 2.89 (t, *J* = 6.1 Hz, 2H, DCC–CH_2), 2.81–2.78 (m, 2H, DCC–CH_2), 2.04–1.98 (m, 4H, N—CH_2—CH and DCC—CH_2), 1.26–1.16 (m, 16H, 4(—CH_2—)), 0.84–0.77 (m, 12H, CH_3). ^{13}C-NMR (125 MHz, CD_2Cl_2, δ ppm): 168.96, 152.41, 146.75, 146.73, 145.82, 145.80, 138.41, 134.67, 130.00, 124.44, 122.46, 120.23, 120.21, 116.98,

116.86, 116.26, 114.97, 114.14, 113.25, 112.20, 74.16, 41.00, 40.90, 30.55, 30.51, 30.46, 29.66, 28.73, 28.65, 28.57, 23.96, 23.93, 23.89, 23.37, 23.35, 23.31, 21.88, 14.05, 14.03, 10.81, 10.76, 10.74, 10.67. HRMS (MALDI-TOF) *m/z*: $[M]^+$ calcd for $C_{37}H_{44}N_4S_3$, 640.27226; found, 640.27138 ($\delta m/m$ = 1.3 ppm).

*2-[3-{7-Formyl-4,5-(di-2-ethylhexyl)-dithieno[2,3-d:2′,3′-d′]thieno[3,2-b:4,5-b′]dipyrrole-2,7-diyl}cyclohex-2-enylidene]malononitrile (**10**)*: Dry DMF (48.0 µL, 0.63 mmol) and $POCl_3$ (57.0 µL, 0.63 mol) were dissolved in 0.5 mL of DCE and stirred for 0.5 h at room temperature. After addition of compound **9** (40.2 mg, 62.7 µmol) dissolved in 2 mL of DCE the reaction mixture was stirred at room temperature for 18 h. The solution was diluted with DCM and hydrolyzed using saturated $NaHCO_3$ solution. The product was extracted with DCM and the combined organic layers were washed with water and dried over Na_2SO_4. After removal of the solvent under reduced pressure, the crude product was purified by column chromatography (SiO_2, DCM/EtOAc = 9:1) to yield product **10** (38.2 mg, 57.1 µmol, 91%) as a dark solid. M_p 241–242 °C. ^{1}H-NMR (400 MHz, CD_2Cl_2, δ ppm): 9.87 (s, 1H, —CHO), 7.68 (s, 1H, Th-β-H), 7.45 (s, 1H, Th-β-H), 7.13 (s, 1H, =CH), 4.39–4.25 (m, 4H, N—CH_2), 2.89 (t, J = 5.9 Hz, 2H, DCC—CH_2), 2.83–2.79 (m, 2H, DCC—CH_2), 2.06–2.00 (m, 4H, N—CH_2—CH and DCC—CH_2), 1.30–1.15 (m, 16H, 4(—CH_2—)), 0.88–0.77 (m, 12H, CH_3). ^{13}C-NMR (125 MHz, CD_2Cl_2, δ ppm): 182.93, 169.05, 152.03, 146.94, 145.47, 140.90, 140.61, 134.44, 132.89, 124.63, 120.44, 117.37, 114.58, 113.78, 113.05, 75.77, 41.03, 30.57, 30.52, 30.50, 30.46, 29.65, 28.75, 28.71, 28.66, 28.64, 28.56, 23.96, 23.36, 23.34, 23.31, 21.82, 14.05, 14.02, 10.80, 10.75, 10.74, 10.69. HRMS (MALDI-TOF) *m/z*: $[M]^+$ calcd for $C_{38}H_{44}N_4OS_3$, 668.26718; found, 668.26622 ($\delta m/m$ = 1.4 ppm). Anal. calcd for $C_{38}H_{44}N_4OS_3$: C 68.22, H 6.63, N 8.37; found: C 68.31, H 6.68, N 8.18.

*2-[3-{7-(Dicyanomethylene)-4,5-(di-2-ethylhexyl)-dithieno[2,3-d:2′,3′-d′]thieno[3,2-b:4,5-b′]dipyrrole-2,7-diyl}cyclohex-2-enylidene]malononitrile (**2**)*: A mixture of **10** (31.9 mg, 47.7 µmol), malononitrile (33.2 mg, 0.50 mmol), and β-alanine (3.90 mg, 43.8 µmol) in 4 mL of DCE:EtOH (1:1) was heated at 70 °C for 20 h. After removal of the solvent the residue was purified by column chromatography (SiO_2, DCM) to afford compound **2** (31.2 mg, 43.5 µmol, 91%) as a green solid. M_p 268 °C (DSC). ^{1}H-NMR (400 MHz, CD_2Cl_2, δ ppm): 7.77 (s, 1H, vinyl-H), 7.62 (s, 1H, Th-β-H)), 7.44 (s, 1H, Th-β-H)), 7.13 (s, 1H, =CH), 4.37–4.24 (m, 4H, N—CH_2), 2.89 (t, J = 5.9 Hz, 2H, DCC—CH_2), 2.83–2.80 (m, 2H, DCC—CH_2), 2.07–1.96 (m, 4H, N—CH_2—CH_2 and DCC—CH_2), 1.31–1.16 (m, 16H, 4(—CH_2—)), 0.86–0.78 (m, 12H, CH_3). ^{13}C-NMR (125 MHz, CD_2Cl_2, δ ppm): 169.01, 151.75, 150.78, 147.76, 147.74, 141.88, 136.34, 132.07, 121.16, 117.92, 115.82, 115.25, 114.41, 113.64, 112.92, 76.44, 71.89, 41.06, 40.96, 30.53, 30.49, 30.47, 30.43, 29.65, 29.62, 28.72, 28.69, 28.64, 28.62, 28.51, 23.95, 23.36, 23.34, 23.32, 23.29, 21.77, 14.06, 14.05, 14.03, 14.02, 10.77, 10.72. HRMS (MALDI-TOF) *m/z*: $[M]^+$ calcd for $C_{41}H_{44}N_6S_3$, 716.27841; found, 716.27723 ($\delta m/m$ = 1.6 ppm). Anal. calcd for $C_{41}H_{44}N_6S_3$: C 68.68, H 6.19, N 11.72, S 13.42; found: C 68.89, H 6.18, N 11.65, S 13.45.

*4,5-(Di-2-ethylhexyl)-2,7-bis(trimethylstannyl)-dithieno[2,3-d:2′,3′-d′]thieno[3,2-b:4,5-b′]dipyrrole (**11**)*: To a solution of 4,5-(di-2-ethylhexyl)-dithieno[2,3-*d*:2′,3′-*d*′]thieno[3,2-b:4,5-*b*′]dipyrrole **4** (224 mg, 0.45 mmol) in 13 mL of dry THF at –78 °C was added *n*-BuLi (1.6 M in *n*-hexane, 0.73 mL, 1.17 mmol) under argon within 30 min. After stirring for 1 h at the same temperature, the mixture was quenched with trimethyltin chloride (286 mg, 1.44 mmol) dissolved in 1.3 mL of THF. The reaction mixture was stirred at the same temperature for 5 min and then overnight at room temperature. After addition of water the product was extracted with Et_2O to provide stannyl derivative **11** as an orange oil (370 mg, 0.45 mmol) in quantitative yield. ^{1}H-NMR (400 MHz, $CDCl_3$, δ ppm): 6.98 (s, 2H, Th-β-H), 4.33–4.19 (m, 4H, N—CH_2), 2.01–1.98 (m, 2H, N—CH_2—CH_2), 1.29–1.14 (m, 16H, 4(CH_2—)), 0.83–0.78 (m, 12H, CH_3), 0.40 (s, 18H, Sn—CH_3). MS (MALDI-TOF) *m/z*: $[M]^+$ calcd for $C_{34}H_{54}N_2S_3Sn_2$, 826.15; found, 826.49 $[M]^+$, 662.48 $[M—SnMe_3]^+$. Compound **11** was used without any further purification.

*3,3′-[4,5-(Di-2-ethylhexyl)-dithieno[2,3-d:2′,3′-d′]thieno[3,2-b:4,5-b′]dipyrrole-2,7-diyl]dicyclohex-2-en-1-one (**12**)*: A mixture of 3-bromocyclohex-2-*en*-1-one **7** (106 mg, 0.61 mmol) and bis-stannylated heteropentacene **11** (217 mg, 0.26 mmol) was dissolved in 5 mL of dry DMF in a schlenk tube and degassed carefully. Then the catalyst $Pd(PPh_3)_4$ (15.2 mg, 13.2 µmol) was added and the reaction mixture was stirred at 80 °C for 18 h. After cooling down to room temperature the solid was filtered and washed with Et_2O to obtain the crude product. The filtrate was reduced under vacuum, extracted with DCM, washed with water, and dried over Na_2SO_4. The solvent was removed under reduced pressure. The combined residue and the filtered solid were purified by column chromatography (SiO_2, DCM:EtOAc = 9:1) to afford diketone **12** (132 mg, 0.19 mmol, 73%) as a red solid. M_p 230 °C (DSC). ^{1}H-NMR (500 MHz, CD_2Cl_2, δ ppm): 7.35 (s, 2H, Th-β-H), 6.38 (s, 2H, =CH), 4.35–4.22 (m, 4H, N—CH_2), 2.85 (t, J = 5.9 Hz, 4H, DCC—CH_2), 2.46–2.43 (m, 4H, DCC—CH_2), 2.19–2.13 (m, 4H, DCC—CH_2), 2.03–1.96 (m, 2H, N—CH_2—CH_2), 1.29–1.15 (m, 16H, 4(—CH_2—)), 0.84–0.77 (m, 12H, CH_3). ^{13}C-NMR (125 MHz, CD_2Cl_2, δ ppm): 198.69, 153.63, 145.87, 145.85, 139.69, 132.20, 121.08, 119.77, 118.70, 118.68 112.19, 40.94, 37.76, 30.47, 30,42, 28.68, 28.60, 28.22, 23.92, 23.88, 23.36, 23.34, 23.01, 14.06, 14.05, 10.76, 10.71. HRMS (MALDI-TOF) *m/z*: $[M]^+$ calcd for $C_{40}H_{50}N_2O_2S_3$, 686.30289; found, 686.30296 ($\delta m/m$ = 0.1 ppm). Anal. calcd for $C_{40}H_{50}N_2O_2S_3$: C 69.93, H 7.34, N 4.08, S 14.00; found: C 70.07, H 7.24, N 4.07, S 13.94.

*2,2′-[3,3′-{4,5-(Di-2-ethylhexyl)-dithieno[2,3-d:2′,3′-d′]thieno[3,2-b:4,5-b′]dipyrrole-2,7-diyl}bis(cyclohex-2-enylidene)]dimalononitrile (**3**)*: Diketone **12** (100 mg, 146 µmol) and malononitrile (80 mg, 1.2 mmol) were dissolved in 12 mL of EtOH:*i*-propanol (2:1) in a Schlenk tube and purged with argon. Then Ti(O-*i*Pr)$_4$ (0.1 mL, 0.3 mmol) was added and the reaction mixture was stirred at 70 °C for 4 d. After 1 d another portion of titanium isopropoxide (0.1 mL, 0.3 mmol) was added. After completion the reaction mixture was diluted with DCM and stirred with 1 M HCl for 1 h. The aqueous phase was removed and the organic phase was washed with saturated $NaHCO_3$ solution and dried over Na_2SO_4. After removal of the solvent the residue was purified by column chromatography (SiO_2, DCM:EtOAc = 9:1) to afford compound **3** (45 mg, 0.05 mmol, 40%) as a green solid. As a byproduct, the mono-reacted compound (45 mg, 0.06 mmol, 42%) was isolated which can be further reacted with malononitrile and Ti(O-*i*Pr)$_4$ to obtain compound **3** in a yield of about 40%. M_p 343 °C (DSC). ^{1}H-NMR (500 MHz, CD_2Cl_2, δ ppm): 7.43 (s, 2H, Th-β-H), 7.10 (s, 2H, =CH), 4.36–4.25 (m, 4H, N—CH_2), 2.89 (t, J = 6.0 Hz, 4H, DCC—CH_2), 2.81–2.79 (m, 2H, DCC—CH_2), 2.05–1.97 (m, 6H, DCC—CH_2 and N—CH_2—CH_2), 1.30–1.16 (m, 16H, 4(—CH_2—)), 0.85–0.78 (m, 12H, CH_3). ^{13}C-NMR (125 MHz, CD_2Cl_2, δ ppm): 168.96, 152.01, 146.86, 146,84, 140.31, 133.18, 121.72, 120.10, 120.08, 117.12, 114.66, 113.86, 113.13, 75.31, 40.98, 30.48, 30.44, 29.61, 28.71, 28.63, 28.48, 23.94, 23.92, 23.37, 23.35, 21.81, 14.08, 14.06, 10.78, 10.73. HRMS (MALDI-TOF) *m/z*: $[M]^+$ calcd for $C_{46}H_{50}N_6S_3$, 782.32536; found, 782.32529 ($\delta m/m$ = 0.09 ppm). Anal. calcd for $C_{46}H_{50}N_6S_3$: C 70.55, H 6.44, N 10.73, S 12.28; found: C 70.42, H 6.57, N 10.69, S 12.11.

Supporting Information

Supporting Information is available from the Wiley Online Library or from the author.

Acknowledgements

The authors thank the German Federal Ministry of Education and Research (BMBF, program LOTsE 03EK3505G) for financial support. M.U. thanks the University of the Basque Country (UPV/EHU) for funding through the EHUA12/05 project.

Received: February 10, 2015
Revised: March 31, 2015
Published online: April 30, 2015

[1] a) B. Walker, C. Kim, T.-Q. Nguyen, *Chem. Mater.* **2011**, *23*, 470; b) J. E. Coughlin, Z. B. Henson, G. C. Welch, G. C. Bazan, *Acc. Chem. Res.* **2014**, *47*, 257; c) *Organic Photovoltaics – Materials, Device Physics and Manufacturing Technologies*, 2nd ed. (Eds: C. Brabec, V. Dyakonov, U. Scherf), Wiley-VCH, Weinheim, Germany **2014**.

[2] a) Y. Liu, C.-C. Chen, Z. Hong, J. Gao, Y. M. Yang, H. Zhou, L. Dou, G. Li, Y. Yang, *Sci. Rep.* **2013**, *3*, 3356; b) V. Gupta, A. K. K. Kyaw, D. H. Wang, S. Chand, G. C. Bazan, A. J. Heeger, *Sci. Rep.* **2013**, *3*, 1965; c) B. Kan, Q. Zhang, M. Li, X. Wan, W. Ni, G. Long, Y. Wang, X. Yang, H. Feng, Y. Chen, *J. Am. Chem. Soc.* **2014**, *136*, 15529; d) K. Sun, Z. Xiao, S. Lu, W. Zajaczkowski, W. Pisula, E. Hanssen, J. M. White, R. M. Williamson, J. Subbiah, J. Ouyang, A. B. Holmes, W. W. H. Wong, D. J. Jones, *Nat. Commun.* **2015**, *6*, 6013.

[3] a) B. Walker, A. B. Tamayo, X.-D. Dang, P. Zalar, J. H. Seo, A. Garcia, M. Tantiwiwat, T.-Q. Nguyen, *Adv. Funct. Mater.* **2009**, *19*, 3063; b) S. Loser, C. J. Bruns, H. Miyauchi, R. P. Ortiz, A. Facchetti, S. I. Stupp, T. J. Marks, *J. Am. Chem. Soc.* **2011**, *133*, 8142; c) H. Shang, H. Fan, Y. Liu, W. Hu, Y. Li, X. Zhan, *Adv. Mater.* **2011**, *23*, 1554; d) W. L. Leong, G. Welch, L. Kaake, C. Takacs, Y. Sun, G. C. Bazan, A. J. Heeger, *Chem. Sci.* **2012**, *3*, 2103; e) G. Long, X. Wan, B. Kan, Y. Liu, G. He, Z. Li, Y. Zhang, Y. Zhang, Q. Zhang, M. Zhang, Y. Chen, *Adv. Energy Mater.* **2013**, *3*, 639; f) J. Zhou, Y. Zuo, X. Wan, G. Long, Q. Zhang, W. Ni, Y. Liu, Z. Li, G. He, C. Li, B. Kan, M. Li, Y. Chen, *J. Am. Chem. Soc.* **2013**, *135*, 8484; g) C. D. Wessendorf, G. L. Schulz, A. Mishra, P. Kar, I. Ata, M. Weidelener, M. Urdanpilleta, J. Hanisch, E. Mena-Osteritz, M. Lindén, E. Ahlswede, P. Bäuerle, *Adv. Energy Mater.* **2014**, *4*, 1400266; h) A. Zitzler-Kunkel, M. R. Lenze, T. Schnier, K. Meerholz, F. Würthner, *Adv. Funct. Mater.* **2014**, *24*, 4645.

[4] A. Zhugayevych, O. Postupna, R. C. Bakus Ii, G. C. Welch, G. C. Bazan, S. Tretiak, *J. Phys. Chem. C* **2013**, *117*, 4920.

[5] a) A. Mishra, P. Bäuerle, *Angew. Chem. Int. Ed.* **2012**, *51*, 2020; b) V. Malytskyi, J.-J. Simon, L. Patrone, J.-M. Raimundo, *RSC Adv.* **2015**, *5*, 354.

[6] a) R. Fitzner, E. Mena-Osteritz, A. Mishra, G. Schulz, E. Reinold, M. Weil, C. Körner, H. Ziehlke, C. Elschner, K. Leo, M. Riede, M. Pfeiffer, C. Uhrich, P. Bäuerle, *J. Am. Chem. Soc.* **2012**, *134*, 11064.

[7] Y. Chen, X. Wan, G. Long, *Acc. Chem. Res.* **2013**, *46*, 2645.

[8] C. Wetzel, A. Mishra, E. Mena-Osteritz, A. Liess, M. Stolte, F. Würthner, P. Bäuerle, *Org. Lett.* **2014**, *16*, 362.

[9] A. Mishra, D. Popovic, A. Vogt, H. Kast, T. Leitner, K. Walzer, M. Pfeiffer, E. Mena-Osteritz, P. Bäuerle, *Adv. Mater.* **2014**, *26*, 7217.

[10] A. Yassin, T. Rousseau, P. Leriche, A. Cravino, J. Roncali, *Sol. Energy Mater. Sol. Cells* **2011**, *95*, 462.

[11] a) Y.-J. Cheng, J.-S. Wu, P.-I. Shih, C.-Y. Chang, P.-C. Jwo, W.-S. Kao, C.-S. Hsu, *Chem. Mater.* **2011**, *23*, 2361; b) Y.-X. Xu, C.-C. Chueh, H.-L. Yip, F.-Z. Ding, Y.-X. Li, C.-Z. Li, X. Li, W.-C. Chen, A. K. Y. Jen, *Adv. Mater.* **2012**, *24*, 6356; c) Y.-L. Chen, C.-Y. Chang, Y.-J. Cheng, C.-S. Hsu, *Chem. Mater.* **2012**, *24*, 3964; d) B. C. Schroeder, R. Ashraf, S. Thomas, A. J. P. White, L. Biniek, C. Nielsen, W. Zhang, Z. Huang, P. Shakya Tuladhar, S. E. Watkins, T. D. Anthopoulos, J. R. Durrant, I. McCulloch, *Chem. Commun.* **2012**, *48*, 7699; e) Z. Fei, R. Ashraf, Z. Huang, J. Smith, R. J. Kline, P. D'Angelo, T. D. Anthopoulos, J. R. Durrant, M. Heeney, I. McCulloch, *Chem. Commun.* **2012**, *48*, 2955; f) C.-A. Tseng, J.-S. Wu, T.-Y. Lin, W.-S. Kao, C.-E. Wu, S.-L. Hsu, Y.-Y. Liao, C.-S. Hsu, H.-Y. Huang, Y.-Z. Hsieh, Y.-J. Cheng, *Chem. - Asian J.* **2012**, *7*, 2102; g) R. S. Ashraf, B. C. Schroeder, H. A. Bronstein, Z. Huang, S. Thomas, R. J. Kline, C. J. Brabec, P. Rannou, T. D. Anthopoulos, J. R. Durrant, I. McCulloch, *Adv. Mater.* **2013**, *25*, 2029.

[12] J. A. Love, I. Nagao, Y. Huang, M. Kuik, V. K. Gupta, C. J. Takacs, J. E. Coughlin, L. Qi, T. S. van der Poll, E. J. Kramer, A. J. Heeger, T.-Q. Nguyen, G. C. Bazan, *J. Am. Chem. Soc.* **2014**, *136*, 3597.

[13] a) K. Staub, G. A. Levina, S. Barlow, T. C. Kowalczyk, H. Lackritz, M. Barzoukas, A. Fort, S. R. Marder, *J. Mater. Chem.* **2003**, *13*, 825; b) K. C. Kreß, T. Fischer, J. Stumpe, W. Frey, M. Raith, O. Beiraghi, S. H. Eichhorn, S. Tussetschläger, S. Laschat, *ChemPlusChem* **2014**, *79*, 223.

[14] R. Fitzner, E. Mena-Osteritz, K. Walzer, M. Pfeiffer, P. Bäuerle, *Adv. Funct. Mater.* **2015**, *26*, 1845.

[15] a) K. Mitsudo, S. Shimohara, J. Mizoguchi, H. Mandai, S. Suga, *Org. Lett.* **2012**, *14*, 2702; b) P. Qin, H. Kast, M. K. Nazeeruddin, S. M. Zakeeruddin, A. Mishra, P. Bäuerle, M. Grätzel, *Energy Environ. Sci.* **2014**, *7*, 2981.

[16] A. Mishra, C. Uhrich, E. Reinold, M. Pfeiffer, P. Bäuerle, *Adv. Energy Mater.* **2011**, *1*, 265.

[17] R. N. Adams, *Electrochemistry at Solid Electrodes*, Marcel Dekker, New York **1969**.

[18] a) J. Peet, J. Y. Kim, N. E. Coates, W. L. Ma, D. Moses, A. J. Heeger, G. C. Bazan, *Nat. Mater.* **2007**, *6*, 497; b) Y. Yao, J. Hou, Z. Xu, G. Li, Y. Yang, *Adv. Funct. Mater.* **2008**, *18*, 1783; c) J. C. Bijleveld, V. S. Gevaerts, D. Di Nuzzo, M. Turbiez, S. G. J. Mathijssen, D. M. de Leeuw, M. M. Wienk, R. A. J. Janssen, *Adv. Mater.* **2010**, *22*, E242; d) T. Salim, L. H. Wong, B. Brauer, R. Kukreja, Y. L. Foo, Z. Bao, Y. M. Lam, *J. Mater. Chem.* **2011**, *21*, 242; e) T.-Y. Chu, J. Lu, S. Beaupré, Y. Zhang, J.-R. Pouliot, S. Wakim, J. Zhou, M. Leclerc, Z. Li, J. Ding, Y. Tao, *J. Am. Chem. Soc.* **2011**, *133*, 4250; f) Y. Kim, H. R. Yeom, J. Y. Kim, C. Yang, *Energy Environ. Sci.* **2013**, *6*, 1909.

[19] a) J. Zhou, X. Wan, Y. Liu, Y. Zuo, Z. Li, G. He, G. Long, W. Ni, C. Li, X.-C. Su, Y. Chen, *J. Am. Chem. Soc.* **2012**, *134*, 16345; b) J. A. Love, I. Nagao, Y. Huang, M. Kuik, V. K. Gupta, C. J. Takacs, J. E. Coughlin, L. Qi, T. S. van der Poll, E. J. Kramer, A. J. Heeger, T.-Q. Nguyen, G. C. Bazan, *J. Am. Chem. Soc.* **2014**, *136*, 3597; c) H. Fan, H. Shang, Y. Li, X. Zhan, *Appl. Phys. Lett.* **2010**, *97*, 133302; d) K. R. Graham, J. Mei, R. Stalder, J. W. Shim, H. Cheun, F. Steffy, F. So, B. Kippelen, J. R. Reynolds, *ACS Appl. Mater. Interfaces* **2011**, *3*, 1210; e) C. J. Takacs, Y. Sun, G. C. Welch, L. A. Perez, X. Liu, W. Wen, G. C. Bazan, A. J. Heeger, *J. Am. Chem. Soc.* **2012**, *134*, 16597; f) Y. Sun, G. C. Welch, W. L. Leong, C. J. Takacs, G. C. Bazan, A. J. Heeger, *Nat. Mater.* **2012**, *11*, 44; g) T. S. van der Poll, J. A. Love, T.-Q. Nguyen, G. C. Bazan, *Adv. Mater.* **2012**, *24*, 3646; h) J. K. Park, C. Kim, B. Walker, T.-Q. Nguyen, J. H. Seo, *RSC Adv.* **2012**, *2*, 2232; i) K. R. Graham, P. M. Wieruszewski, R. Stalder, M. J. Hartel, J. Mei, F. So, J. R. Reynolds, *Adv. Funct. Mater.* **2012**, *22*, 4801; j) H. Wang, F. Liu, L. Bu, J. Gao, C. Wang, W. Wei, T. P. Russell, *Adv. Mater.* **2013**, *25*, 6519; k) Y. Liu, Y. Yang, C.-C. Chen, Q. Chen, L. Dou, Z. Hong, G. Li, Y. Yang, *Adv. Mater.* **2013**, *25*, 4657; l) M. T. Dang, J. D. Wuest, *Chem. Soc. Rev.* **2013**, *42*, 9105.

[20] S. Haid, A. Mishra, C. Uhrich, M. Pfeiffer, P. Bäuerle, *Chem. Mater.* **2011**, *23*, 4435.

[21] R. Fitzner, E. Reinold, A. Mishra, E. Mena-Osteritz, H. Ziehlke, C. Körner, K. Leo, M. Riede, M. Weil, O. Tsaryova, A. Weiß, C. Uhrich, M. Pfeiffer, P. Bäuerle, *Adv. Funct. Mater.* **2011**, *21*, 897.

[22] J. C. Hummelen, B. W. Knight, F. LePeq, F. Wudl, J. Yao, C. L. Wilkins, *J. Org. Chem.* **1995**, *60*, 532.

[23] a) L. J. A. Koster, V. D. Mihailetchi, R. Ramaker, P. W. M. Blom, *Appl. Phys. Lett.* **2005**, *86*, 123509; b) C. J. Brabec, A. Cravino, D. Meissner, N. S. Sariciftci, T. Fromherz, M. T. Rispens, L. Sanchez, J. C. Hummelen, *Adv. Funct. Mater.* **2001**, *11*, 374.

[24] a) M. C. Scharber, D. Mühlbacher, M. Koppe, P. Denk, C. Waldauf, A. J. Heeger, C. J. Brabec, *Adv. Mater.* **2006**, *18*, 789;

b) R. A. J. Janssen, J. Nelson, *Adv. Mater.* **2013**, *25*, 1847.
[25] G. Wei, S. Wang, K. Sun, M. E. Thompson, S. R. Forrest, *Adv. Energy Mater.* **2011**, *1*, 184.
[26] J. Liu, B. Walker, A. Tamayo, Y. Zhang, T.-Q. Nguyen, *Adv. Funct. Mater.* **2013**, *23*, 47.
[27] G. Long, X. Wan, B. Kan, Y. Liu, G. He, Z. Li, Y. Zhang, Y. Zhang, Q. Zhang, M. Zhang, Y. Chen, *Adv. Energy Mater.* **2013**, *3*, 639.
[28] H. Bürckstümmer, E. V. Tulyakova, M. Deppisch, M. R. Lenze, N. M. Kronenberg, M. Gsänger, M. Stolte, K. Meerholz, F. Würthner, *Angew. Chem. Int. Ed.* **2011**, *50*, 11628.
[29] a) J. Roncali, P. Leriche, P. Blanchard, *Adv. Mater.* **2014**, *26*, 3821; b) Y. Zhang, X. Bao, M. Xiao, H. Tan, Q. Tao, Y. Wang, Y. Liu, R. Yang, W. Zhu, *J. Mater. Chem. A* **2015**, *3*, 886.
[30] I. Horcas, R. Fernández, J. M. Gómez-Rodríguez, J. Colchero, J. Gómez-Herrero, A. M. Baro, *Rev. Sci. Instrum.* **2007**, *78*, 013705.